Synthesis, crystal structure, Hirshfeld surfaces, and thermal, mechanical and dielectrical properties of cholest-5-ene

Shamsuzzaman [a,*], Hena Khanam [a,1], Ashraf Mashrai [a,1], Mohd Asif [a], Abad Ali [a], Assem Barakat [b,c], Yahia N. Mabkhot [b]

[a] *Steroid Research Laboratory, Department of Chemistry, Aligarh Muslim University, Aligarh 202002 (UP), India*
[b] *Department of Chemistry, Faculty of Science, King Saud University, Riyadh 11451, Saudi Arabia*
[c] *Department of Chemistry, Faculty of Science, Alexandria University, Alexandria 21321, Egypt*

Abstract

The title compound derived from 3β-chlorocholest-5-ene has been synthesized and characterized successfully. A single crystal X-ray investigation of the compound revealed that the van der Waals interactions play a key role in the formation of the elementary structure. Hirshfeld surface analysis was used to visualize the fidelity of the crystal structure. This method permitted the identification of individual types of intermolecular contacts and their impact on crystal packing. Molecules are linked by a combination of C—H···H and C···H contacts, which have clear signatures in the fingerprint plots. The absorption spectrum exhibited a strong absorption band of approximately 246 nm, and the fluorescence spectrum of the compound showed one broad peak at 367 nm. Thermal studies established that the compound undergoes no phase transition and is stable up to 200 °C. The hardness of the grown crystal increases as the load increases. The electric permittivity of cholest-5-ene decreases with increasing frequency and becomes almost constant at high frequencies.

1. Introduction

Recently, research has focused on the development of organic solids that have physical properties that make them usable for smart materials and artificial molecular machines [1]. Steroid chemistry has been extensively studied, and steroids can be functionalized at several points along their four ring structures [2]. Steroids have been used in hybrid materials with wide applications [3]. These applications include steroid-doped liquid crystalline polymers, functionalized-nanotubes, and gels; therefore, the use of steroidal compounds in materials science has been gradually increasing concomitant with advancements in materials science [4–6]. Steroidal structures are uniquely valuable to crystal engineering, which takes advantage of their tendency to adopt different crystal forms [7]. In addition, steroids constitute an important class of biologically active polycyclic compounds that are extensively used for therapeutic purposes

---

* Corresponding author. Tel.: +91 9411003465.
  E-mail address: shamsuzzaman9@gmail.com (Shamsuzzaman).
[1] These authors have contributed equally.
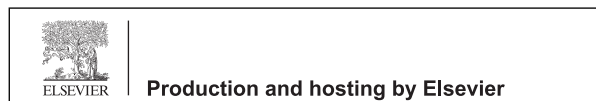
[8,9]. Despite decades of research, the total synthesis of steroid nuclei continues to receive considerable attention. Steroids are widely distributed in nature and possess practical medical importance. Steroids are a preferred testing ground for the development of more efficient methods for organic synthesis [10]. The methods for synthesizing steroids have focused on key transformations, including alteration of the configuration of a stereocenter, aromatization of a ring, incorporation of a heteroatom and annulation of a heterocyclic ring. By making structural modifications, the physiological activity of a compound can be changed [11–15].

The application of Hirshfeld surface analysis is increasing in the field of crystallography. This approach is a convenient tool for the investigation of intermolecular interactions. Because the crystal structure provides the most definite understanding of the intermolecular contacts and crystal packing of a compound, Hirshfeld surface [16a] based tools appear to be particularly suitable for visualizing variations in the intermolecular interactions of compounds. The breakdown of the associated fingerprint plots [16b] provides a quantitative analysis of the types of intermolecular contacts that are present in a molecule and presents this information in a colour plot. The present structure is similar to cholest-5-ene [17]. In continuation of our research on the synthesis of steroids and single crystal X-ray analysis [18], we report herein a structural analysis of cholest-5-ene single crystals. We obtained crystal data by performing growth, spectral, optical, thermal, mechanical and dielectrical studies; Hirshfeld surfaces and fingerprint plots were also analyzed. Notably, an earlier report [17] did not provide any information regarding intermolecular contacts; however, in the present study, we explored short intermolecular contacts by Molecular Hirshfeld Surfaces.

2. Experimental

2.1. Materials and measurements

All reagents and solvents were commercially available and used as received. The melting point of the compound was determined on a digital auto melting point apparatus. Elemental analysis of the compound was recorded on a Perkin Elmer 2400 CHN Elemental Analyzer. The IR spectrum of the compound was recorded on KBr pellets with Spectrum Two with a Perkin Elmer Spectrometer, and values are given in cm^{-1}. ^{1}H and ^{13}C NMR spectra were run in CDCl$_3$ on a Bruker Avance II 400 NMR Spectrometer at 400 MHz and 100 MHz, respectively. Chemical shifts (δ) are reported in ppm relative to TMS (^{1}H NMR, 400 MHz)

and the solvent signal (^{13}C NMR spectra, 100 MHz); coupling constants are given in Hz. A NANOPHOXTM particle size analyser was used for measuring the particle size. The surface morphology of the compound was monitored using a JEOL JSM-6510LV scanning electron microscope (SEM) equipped with an energy-dispersive X-ray spectroscopy (EDX) analyser. The thermal study of the compound was carried out using a TGA/DTA-60H and DSC-60 instrument (SHIMADZU) at a heating rate of 20 °C/min from ambient temperature to 800 °C (for DSC 500 °C). The UV–visible spectrum was recorded on a UV-Vis spectrophotometer (Perkin Elmer Life and Analytical Sciences, CT, USA) over the wavelength range of 200–700 nm. The fluorescence spectrum was collected at 37 °C with a 1-cm path-length cell using a Hitachi spectrofluorometer (Model 2500) equipped with a PC; the emission slit was set at 5 nm. The emission spectrum was recorded in the range of 330 to 400 nm. The dielectric property was determined using impedance spectroscopy. The powder was pressed into pellets that had a 13-mm diameter and 0.84-mm thickness. A dielectric spectroscopy measurement was carried out in the frequency range of 1 kHz to 1 MHz using a LCR metre (Agilent 48). The pellets were coated on adjacent faces with silver paste, thereby forming parallel plate capacitor geometry. The value of the dielectric constant (ε) was calculated using the following formula: $\varepsilon = cp \cdot d / \varepsilon_o A$, where ε_o = permittivity of free space, d = thickness of pellet, A = cross sectional area of the flat surface of the pellet, and cp = capacitance of the specimen in Farad (F).

2.2. X-ray diffraction study

Three-dimensional intensity data of cholest-5-ene were collected at 100 K on a Bruker KAPPA APEXII DUO diffractometer using Cu Kα radiation (λ = 1.54178 Å). The structure was solved by direct methods using SHELXS-97 software (SHELDRICK, 1990). Isotropic refinement of the structure by least-squares methods was carried out using SHELXL-97 (SHELDRICK, 1997) followed by anisotropic refinement on F^2 for all of the non-hydrogen atoms. All non-hydrogen atoms were refined anisotropically. Crystallographic data (excluding structure factors) for the structures reported in this article were deposited with the Cambridge Crystallographic Data Centre (CCDC) as deposition no. CCDC 895768. All of the H-atom positions were calculated geometrically with Uiso (H) = 1.2–1.5 Å Ueq (parent atom). A riding model was used in their refinement (C−H = 0.98–1.00 Å). The X-ray diffraction (PXRD) pattern of the powdered sample

was recorded on a MiniFlex[TM] II benchtop XRD system (Rigaku Corporation, Tokyo, Japan) operating at 40 kV and a current of 30 mA with Cu Kα radiation (λ = 1.54 Å). The diffracted intensities were recorded from 20° to 80° 2θ angles with a scan rate of 2°/min and a step size of 0.02°, and measurements were performed at ambient temperature.

2.3. Molecular Hirshfeld surfaces calculations

Molecular Hirshfeld surfaces calculations were performed using the CRYSTALEXPLORER [19] program. When the cif file of the title compound was entered into the CRYSTALEXPLORER program, all of the bond lengths to hydrogen were automatically modified to the standard neutron values (C—H = 1.083 Å). The 2D fingerprint plots were produced using the standard 0.6–2.6 Å view with the *de* and *di* distance scales displayed on the graph axes.

2.4. Synthesis of cholest-5-ene

Caution! *Care must be taken while using sodium, as it generates flammable hydrogen and caustic sodium hydroxide upon contact with water.*

3β-Chlorocholest-5-ene (10 g) was dissolved in warm amyl alcohol (230 mL). Sodium metal (20 g) was added to the solution in small portions with continuous stirring over a period of 8 h. The reaction mixture was warmed occasionally. When sodium metal was completely dissolved, methanol was added and the resultant mixture was poured into water, acidified with dilute HCl and then allowed to stand overnight. The crystalline solid thus obtained was filtered under suction, washed thoroughly with water and air-dried. The crude material was recrystallized from acetone to provide cholest-5-ene, m.p. 88–89 °C (reported m.p. 89–91 °C) [20] (Scheme 1).
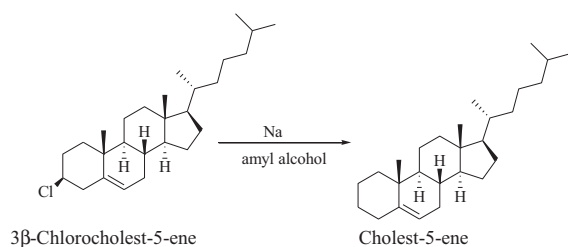
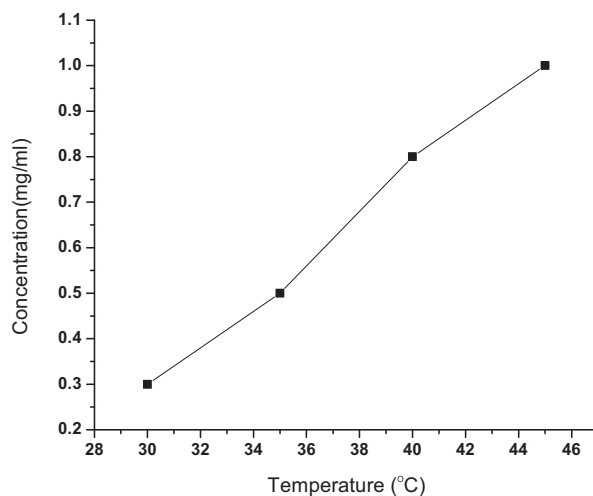Scheme 1. Synthesis of cholest-5-ene.

Fig. 1. Solubility curve of cholest-5-ene in acetone.

3. Results and discussion

The present structure is similar to the previously reported cholest-5-ene [16]. Here, we obtained new characterization data regarding this compound that have not been previously disclosed.

3.1. Solubility and crystal growth studies

Selection of a suitable solvent is crucial for the growth of good quality single crystals. Equilibrium solubility and its temperature dependence are essential factors for solution growth. The data from the solubility curve are sufficient to start growing fair quality single crystals. The solubility of cholest-5-ene in acetone was assessed as a function of temperature in the temperature range of 30–45 °C. The amount of cholest-5-ene required to make a saturated solution at different temperatures was estimated gravimetrically; the obtained solubility curve is shown in Fig. 1. The solubility curve shows that the compound exhibits a positive solubility-temperature gradient, which is an important factor for growing good quality crystals from solution. The saturated solution of cholest-5-ene (approximately 50 mL) was prepared in acetone according to the solubility curve. Then, the prepared solution was passed through anhydrous sodium sulphate, covered with aluminium foil and left at room temperature. After a few days, colourless crystals of cholest-5-ene were obtained.

3.2. Elemental analysis

An analysis of carbon and hydrogen was carried out to ascertain the constituents and purity of the synthesized

compound. Elemental analysis of $C_{27}H_{46}$ calculated C = 87.49% and H = 12.51% and found C = 87.69% and H = 12.30%. The experimental and calculated values matched $\pm0.4\%$; the purity of the compound was >95%.

3.3. FT-IR spectral analysis

Infrared spectroscopy is used to identify the functional groups and modes of vibration of the synthesized compound (Fig. S1). The peaks at 1376 and 1462 cm^{-1} corresponded to symmetric and asymmetric bends of the C–H group, respectively. The characteristic bands in the range of 2864 to 2933 cm^{-1} were ascribed to C–H stretching vibrations, while the band at 1625 cm^{-1} was ascribed to C=C.

3.4. NMR spectroscopy

The ^{1}H NMR, ^{13}C NMR and DEPT studies confirmed the molecular structure of cholest-5-ene. The ^{1}H NMR spectrum provides useful information about the number of unique types of protons and also the nature of the immediate environment of each of them. The ^{1}H NMR spectrum (Fig. S2) of the title compound showed the expected signals of cholestane nuclei [21] and a distinguishing triplet attributed to one olefinic (C6-H) proton at 5.26 (J = 2.32, 2.8 Hz). The ^{13}C NMR spectrum (Fig. S3) showed signals at 143.68 and 119.02 ppm, which are attributed to C-5 and C-6, respectively. The nature of each carbon in the compound was deduced through a Distortionless Enhancement by Polarization Transfer (DEPT) (Fig. S4) experiment using polarization pulses of 135°, obtaining positive signals (up) for CH and CH$_3$ and negative signals (down) for CH$_2$ groups. The DEPT (135) revealed the presence of five sp^3 methyl carbons, twelve sp^3 methylene carbons and seven methine (six sp^3 and one sp^2) carbons.

3.5. Description of crystal structure

The title compound crystallizes in the monoclinic system, space group $P2_1$, which can be explained by the presence of 7 *chiral* centres [22]. There are two molecules in the asymmetric unit, while the unit cell contains 4 molecules with lattice constants of a = 10.7321(4) Å, b = 19.4426(7) Å, and c = 11.1735(4) Å; the detailed data are listed in Tables 1 and 2. Fig. 2 shows ortep and 2D views of the compound. The solvent molecule was not located in discrete locations in the crystal structure. The three six-membered rings are all in chair conformations, and ring D is an 11β envelope. The A/B ring junction was

Table 1
Crystal data and structure refinement of cholest-5-ene.

Empirical formula	$C_{27}H_{46}$
Formula weight	370.64
Wavelength (λ)	1.54178 Å
Crystal system	Monoclinic
Space group	$P\,21$
Unit cell dimensions	
a, Å	10.7321(4)
b, Å	19.4426(7)
c, Å	11.1735(4)
α (deg)	90.00
β (deg)	93.517(3)
γ (deg)	90.00
Volume, Å^3	2327.07(15)
No. of molecules per unit cell (Z)	4
Calculated density, Mg m^{-3}	1.058
Absorption coefficient (μ, mm^{-1})	0.422
$F(0\,0\,0)$	832
Crystal size	$0.25 \times 0.21 \times 0.13$ mm
θ range for data collection	3.96–66.39
Limiting indices	$-12 <= h <= -12,$ $-23 <= k <= 22,$ $-12 <= l <= 12$
Reflections collected	7722
Restraints/parameters	1/498
Goodness-of-fit on F^2	1.052
Final R indices [$I > 2\sigma(I)$]	$R1 = 0.0383, wR2 = 0.0967$
R indices (all data)	$R1 = 0.0427, wR2 = 0.0991$

$R1 = \Sigma||Fo| - |Fc||/\Sigma|Fo|$ with $\qquad$ Fo$^2 > 2\sigma$(Fo^2).
$wR2 = [\Sigma w(|Fo^2| - |Fc^2|)^2/\Sigma|Fo^2|^2]^{1/2}$.

Table 2
Selected bond lengths (Å) and angles (deg) for cholest-5-ene.

Bond lengths	
C2B–C3B	1.507(3)
C6B–C7B	1.552(2)
C7B–C8B	1.562(2)
C1B–C17B	1.492(3)
C16B–C17B	1.536(2)
C11B–C15B	1.543(2)
Bond angles	
C1B C2B C3B	120.48(17)
C3B C2B C7B	116.35(15)
C6B C7B C8B	108.80(14)
C2B C1B C17B	124.95(16)
C15B C16B C17B	110.70(14)
C15B C16B C8B	109.80(14)

quasi-trans, while the B/C and C/D ring systems were *trans*-fused about the C(8)–C(16) and C(11)–C(15) bonds. The ring bond lengths have normal values, with an average of 1.528(3) Å, while the cholestane side chain shows an average bond length of 1.521(3) Å. The bond length for C(1)–C(2) was 1.340(3) Å, which indicates a double-bond character [23]. The side-chain was fully
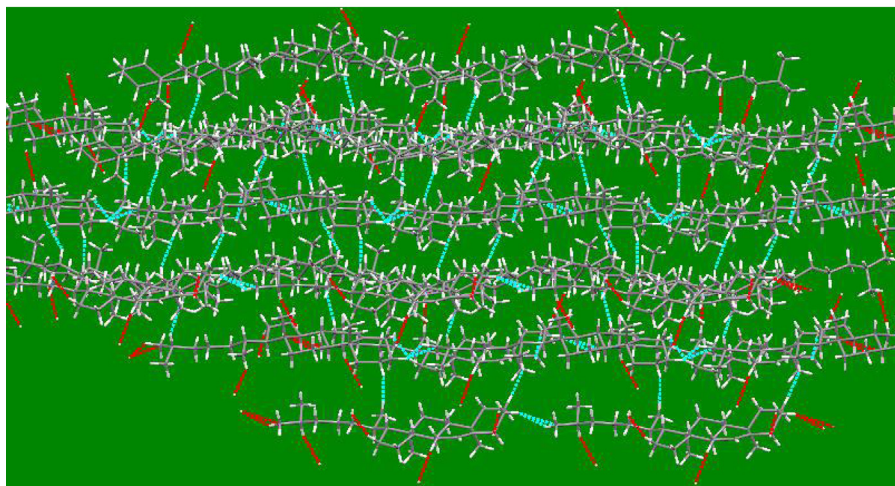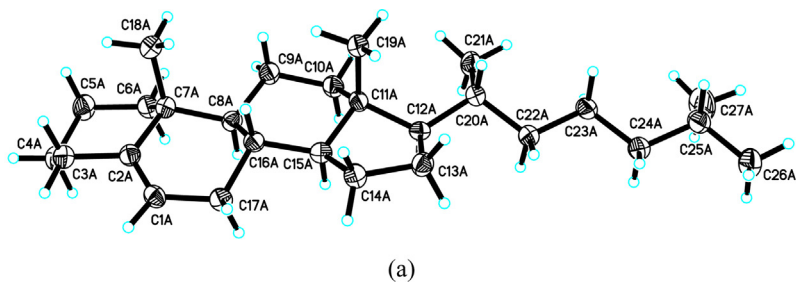
(a)

(b)

Fig. 2. 2D view of cholest-5-ene.

extended with a *gauche-trans* conformation of the terminal C26 and C27 methyl groups. The H atom on C20 was in the back next to C19 in the crystal structure, and C22 was found to be *trans*-oriented to C11. There are seven *chiral* centres in the molecule; the absolute configuration of these sites was as follows: C7 = *R*, C8 = *S*, C11 = *S*, C12 = *R*, C15 = *S*, C16 = *S* and C20 = *R*. Due to the paucity of hydrogen-bonds, the crystalline molecule interacts through only van der Waals interactions. It is useful to know the relation between morphological variations and the growth parameters, which extends to applied fields, including pharmaceuticals, quality control of optoelectronic crystals and industrial crystallization. The morphology of cholest-5-ene crystal was predicted using WinXMorph program [24,25], and it is depicted in Fig. 3. The morphology of cholest-5-ene revealed four well-developed facets, including (123), (010), (0$\bar{1}\bar{1}$), ($\bar{1}\bar{1}$1). The morphology of the grown crystal (Fig. 3) shows that the (0$\bar{1}\bar{1}$) facet has a larger surface area than the other three facets. The angles between the facets (123)–($\bar{1}\bar{1}$1), (123)–(0$\bar{1}\bar{1}$) and (0$\bar{1}\bar{1}$)–(010) were 77.42°, 160.139° and 119.839°, respectively.
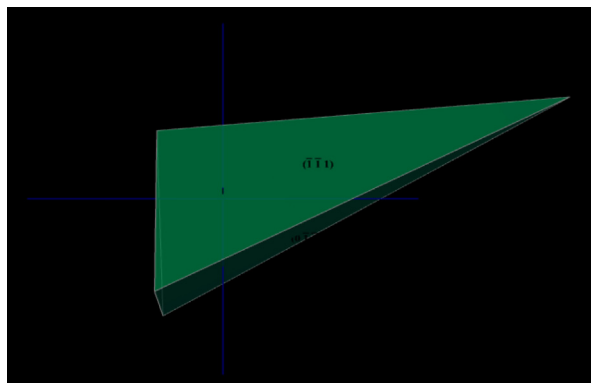

Fig. 3. Equilibrium morphology of a cholest-5-ene single crystal.

3.6. Molecular Hirshfeld surfaces

The Hirshfeld surface is a useful tool for describing the surface characteristics of molecules. The molecular Hirshfeld surfaces of cholest-5-ene were generated using a standard (high) surface resolution with the 3D d_{norm} surfaces mapped over a fixed colour scale of −0.22 (red) to 1.4 Å (blue). The *shape index* mapped in the
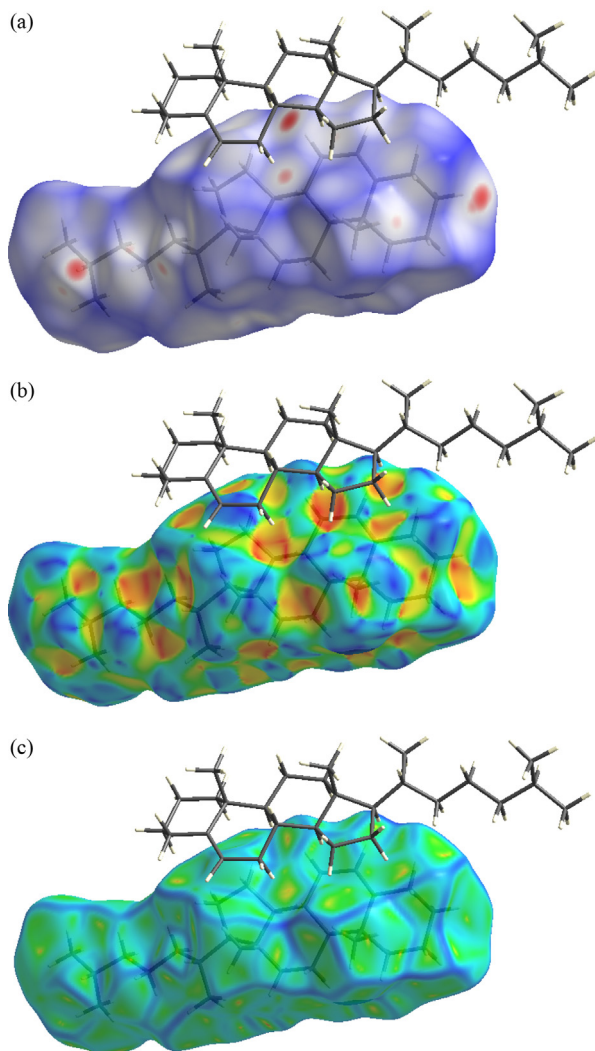
(a)

(b)

(c)

Fig. 4. Hirshfeld surfaces of cholest-5-ene: (a) 3D d_{norm} surface, (b) *surface index*, (c) *curvedness*.

colour range of -0.99 to 1, and *Curvedness* was in the range of 4.0–0.4. The surfaces were shown to be transparent to allow visualization of the molecular moiety in a similar orientation for all of the structures, around which they were calculated. The molecular Hirshfeld surface (d_{norm}, *Shape index* and *Curvedness*) of cholest-5-ene is shown in Fig. 4. The 3D d_{norm} surface was used for to identify very close intermolecular interactions. The value of d_{norm} was negative or positive when intermolecular contacts were shorter or longer than r^{vdW} [van der Waals (vdW) radii], respectively. The d_{norm} values were mapped onto the Hirshfeld surface using a red-blue-white colour scheme as follows: red regions represented closer contacts and a negative d_{norm} value; blue regions represented longer contacts and a positive

d_{norm} value; and white regions represented the distance of contacts equal to exactly the vdW separation with a d_{norm} value of zero. The *shape index* is highly sensitive to very subtle changes in the surface shape; the information conveyed by the *shape index* are consistent with 2D fingerprint plots. The *curvedness* is the measurement of "how much shape" there is in a crystal. The flat areas of the surface correspond to low values of *curvedness*, whereas sharp curvature areas correspond to high values of *curvedness* and usually tend to divide the surface into patches, indicating interactions between neighbouring molecules. The 2D fingerprint plots can be deconstructed to highlight particular atom pair contacts. This deconstruction enables the separation of contributions from different interaction types that overlap in the full fingerprint. The Hirshfeld surface analysis of the molecule showed H···H and C···H interactions of 98.6 and 1.4%, respectively, which revealed that the main intermolecular interactions were H···H intermolecular interactions. The C···H/H···C interactions were represented by a small area in the top left and bottom right side, whereas the H···H interactions were represented by the largest region in the fingerprint plot (Fig. 5) ($d_i = 1.793$ Å, $d_e = 1.578$ Å) and thus had the most significant contribution to the total Hirshfeld surfaces (98.6%).

3.7. Powder XRD

The powder XRD pattern of cholest-5-ene is shown in Fig. S5. The XRD profiles showed that the grown crystal was of a single phase without detectable impurities. The appearances of sharp and strong peaks confirmed the good crystallinity of the grown crystals. The lattice parameters of the crystals were calculated theoretically using the powder XRD data and were in good agreement with the values obtained from single crystals.

3.8. Density measurement

The calculated density of $C_{27}H_{46}$ was measured by the ratio of the cell mass to the cell volume; the equation used to calculate the density is $\rho_{calc} = MZ/NV$, where M is the chemical formula weight of $C_{27}H_{46}$, Z is the number of formula units in one cell, N is Avogadro's number and V is the volume of the unit cell. According to the crystallographic data, it was observed that $a = 10.7321(4)$ Å, $b = 19.4426(7)$ Å, $c = 11.1735(4)$ Å, M = 370.64, Z = 4, and V = 2327.07(15) Å^3. Therefore, the calculated density of the $C_{27}H_{46}$ crystal was found to be 1.058 Mg/m^3. The experimentally calculated density of the cholest-5-ene crystal was measured using the buoyancy method
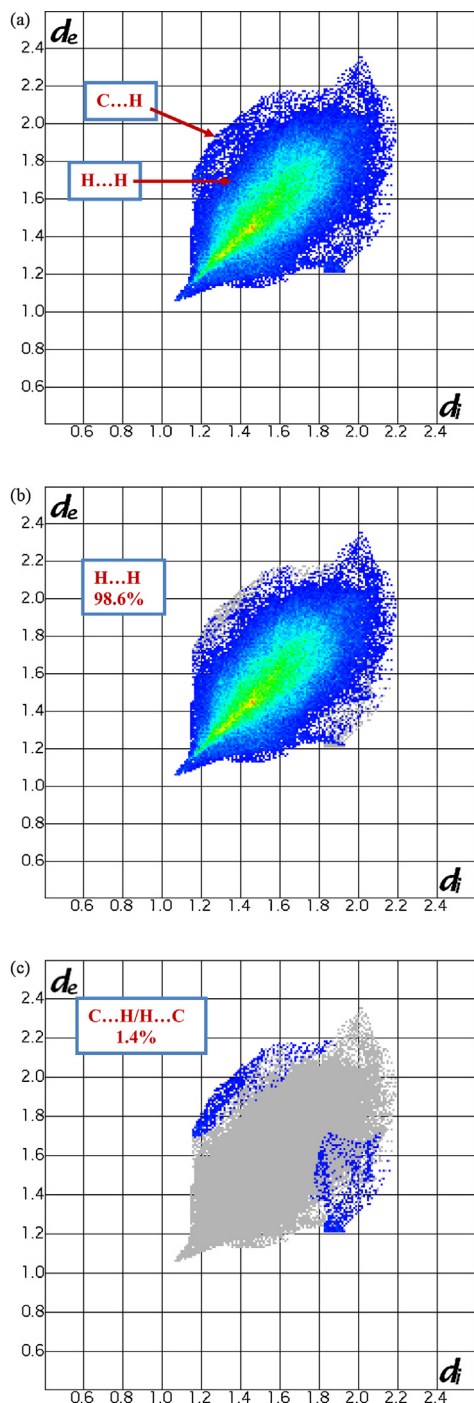
Fig. 5. 2D fingerprint plots of cholest-5-ene: (a) full and (b) resolved into H···H and (c) C···H/H···C contacts, showing the percentages of contacts contributing to the total Hirshfeld surface area of the molecule.

at room temperature (22 °C) in silicon oil. The experimental density of the as-grown $C_{27}H_{46}$ crystal at 22 °C was $1.056 \pm 0.002\,Mg\,m^{-3}$, which is almost equal to the calculated density.

3.9. Deliquescence test

To test the deliquescence of the cholest-5-ene crystal, the crystal sample was exposed to air at room temperature. At the beginning, the crystal sample was transparent and the weight was approximately 0.8812 g. After five days, there was no change in the weight (0.8813 g). Even after 15 days, no change in the weight (0.8815 g) was found. These observations indicate that the cholest-5-ene crystal has good deliquescence resistance and is stable to air.

3.10. Particle size analyser

The particle size was analyzed using laser diffraction in which the sample was mixed with distilled water using Ultrasonic centrifugation. The average particle size of cholest-5-ene was 400 nm, as shown in Fig. 6.

3.11. Scanning electron microscopy/energy-dispersive X-ray spectroscopy (SEM/EDX)

The recorded SEM image of cholest-5-ene is shown in Fig. 7. The SEM micrograph showed brick-shaped cholestene particles, with few microcrystals. Energy dispersive X-ray spectrometry (EDX) provided crystalline information at the nanometre depth of the material surface [26], and EDX analysis (Fig. S6) of the grown crystal depicted the presence of C.

3.12. Optical properties (absorption spectra/fluorescence spectra)

UV–visible spectroscopy is one of the best techniques to determine the suitability of grown crystals for optical device fabrications. The UV–visible absorption properties of cholest-5-ene were recorded in a dichloromethane solution with a concentration of 10^{-5} M. The absorption spectrum (Fig. 8) exhibited a strong, featureless absorption band at approximately 246 nm, which can be assigned to an allowed $\pi \rightarrow \pi^*$ transition of the C=C double bond. Fig. 9 shows a fluorescence image of the compound which indicated one broad peak at 367 nm.

3.13. Thermal stability of cholest-5-ene

Thermogravimetric/differential thermal analysis/differential scanning calorimetry (TG/DTA/DSC) measurements were performed under a nitrogen atmosphere to examine the thermal stabilities of the crystalline sample and to define the conditions for
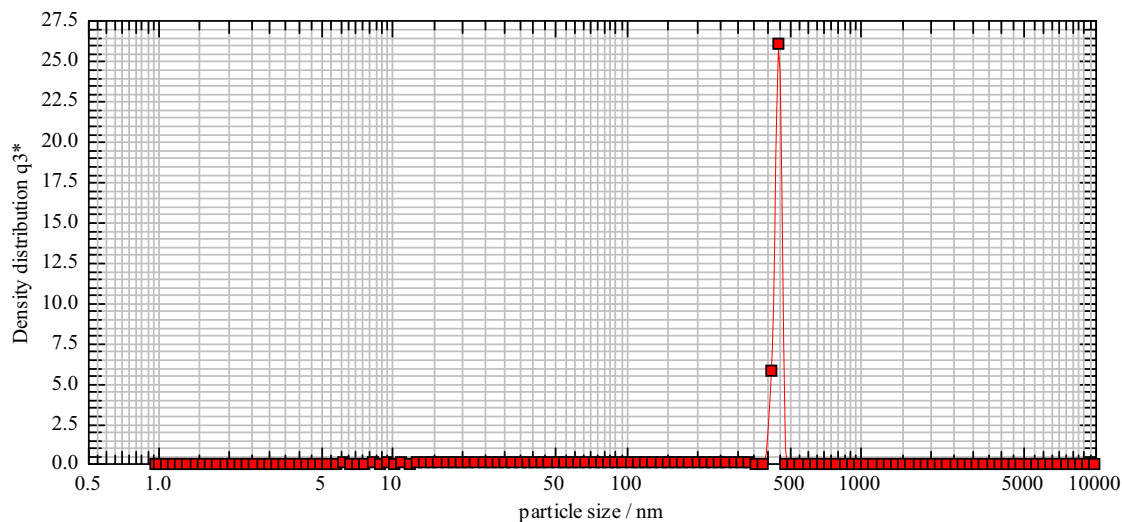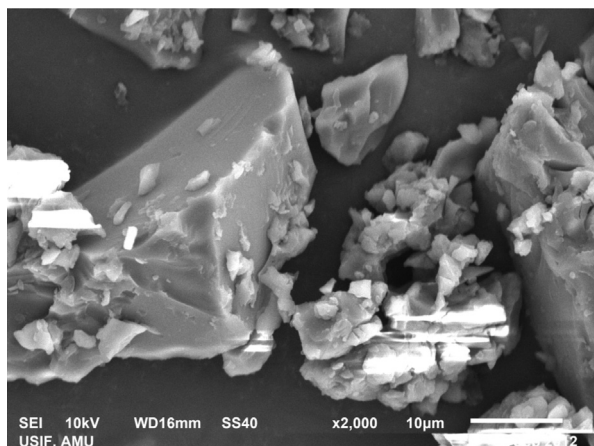
Fig. 6. Particle size analyser of cholest-5-ene.

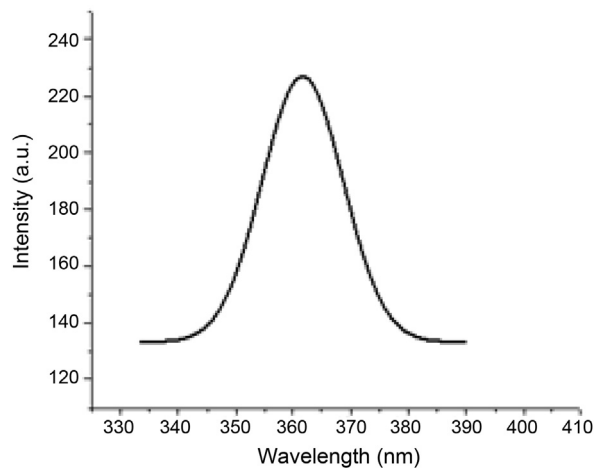Fig. 7. SEM micrograph of cholest-5-ene.

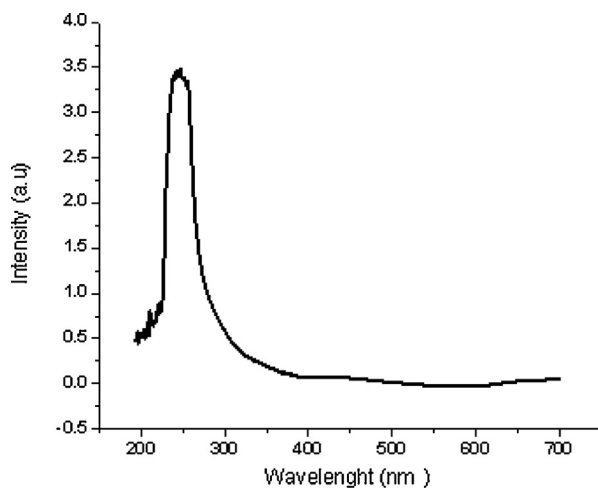Fig. 9. Fluorescence spectrum of cholest-5-ene.

Fig. 8. UV–vis spectrum of cholest-5-ene.

the thermal treatment. The thermograms observed from simultaneous TG/DTA/DSC are illustrated in Figs. S8–S10. The TGA curve of cholest-5-ene revealed that it was stable up to 200 °C (no weight loss) and did not undergo any phase transition. After 200 °C, it started to decompose, and a 69.89% weight loss occurred at 316 °C. At 506 °C, 30.51% of the mass was lost. The disintegration process continued with the confiscation of almost all of the fragments as gaseous products, leading to the bulk decomposition of the compound. At 650 °C, all of the mass was lost and nothing was left as residue. The absence of any weight loss or phase transition around or before the crystal's melting point confirmed the nonexistence of any lattice entrapped solvent or moisture on the grown material,

as well as the high stability of the steroidal compound. The corresponding DTA curve showed three notable exothermic peaks at 163, 399 and 561 °C. From the DSC (differential scanning calorimetry) curve, the melting point was found to be 88–89 °C.

3.14. Mechanical studies

Transparent crystals without cracks were selected for microhardness measurements. The crystals were carefully lapped and washed to avoid surface defects. Vickers hardness indentations were made on the as-grown surface of the cholest-5-ene at room temperature, with a load ranging from 5 to 50 g, keeping the time of indentation at 10 s for all trials [27]. The Vickers hardness number, H_v, was calculated from the following equation:

$$H_v = 1.8544 P/d^2 \text{ kg mm}^{-2};$$

where P is the applied load in kilograms and d is the mean diagonal length of the indentation impression in micrometres. Our results indicate that the hardness of the grown crystal increases as the load increases (Fig. S11). The samples could not withstand loads above 50 g. This may be a result of the internal stresses released during the indentation.

3.15. Dielectrical properties

The dielectric properties of the crystal were measured as a function of frequency at room temperature by equation $\varepsilon^* = \varepsilon - i\varepsilon''$, where ε is the real part of the dielectric constant that describes the stored energy and ε'' is the imaginary part of the dielectric constant that describes the dissipated energy. The dielectric property is shown in Fig. S12. As the frequency increases, the electric permittivity decreases and becomes almost constant at high frequencies. This behaviour can be explained using the Maxwell–Wagner interfacial model. According to this model, a dielectric medium is considered to be composed of double layers, well-conducting grains, which are separated by poorly conducting or resistive grain boundaries. Under the application of an external electric field, the charge carriers can easily migrate the grains, but accumulate at the grain boundaries. This process can produce large polarizations and high electric permittivity. The higher value of electric permittivity can also be explained on the basis of interfacial/space charge polarization due to the nonhomogeneous dielectric structure.

4. Conclusion

Cholest-5-ene, a derivative of the cholestane family, was synthesized and characterized successfully. Elemental analysis, FT-IR, ^{1}H NMR, ^{13}C NMR and DEPT studies confirmed the molecular structure. The structure was solved and refined in the monoclinic space group $P2_1$; the unit cell parameters were $a = 10.7321(4)$ Å, $b = 19.4426(7)$ Å, $c = 11.1735(4)$ Å, $\alpha = 90°$, $\beta = 93.517(3)°$, and $\gamma = 90°$. The powder X-ray diffraction (PXRD) of the compound was recorded to ascertain the phase homogeneity. Molecular Hirshfeld surfaces revealed that the compound was supported mainly by H···H and C···H intermolecular interactions. The fingerprint plots identified the types of intermolecular interactions present in the title crystal. The compound exhibited an absorption maximum at 246 nm, and the emission spectrum exhibited a maximum at 367 nm. According to the thermal analyses, cholest-5-ene is stable from room temperature up to 200 °C. The dielectrical studies showed that the electric permittivity decreases with increasing frequency.

Appendix A. Supplementary data

Supplementary data associated with this article can be found, in the online version, at doi:10.1016/j.jtusci.2016.01.001.

References

[1] A. Comotti, S. Bracco, P. Valsesia, M. Beretta, P. Sozzani, Angew Chem. Int. Ed. 49 (2010) 1760–1764.
[2] J. Fried, J.A. Edwards, Organic Reactions in Steroid Chemistry, vol. I, Van Nostrand Reinhold Company, New York, USA, 1972.
[3] Nonappa, U. Maitra, Org. Biomol. Chem. 6 (2008) 657–669.
[4] B.G. Du, J.S. Hu, B.Y. Zhang, L.J. Xiao, K.Q. Wei, J. Appl. Polym. Sci. 102 (2006) 5559–5565.
[5] P. Terech, A. de Geyer, B. Struth, Y. Talmon, Adv. Mater. 14 (2002) 495–498.
[6] N. Fujita, S. Shinkai, Design and function of low molecular-mass organic gelators bearing steroid and sugar groups, in: Molecular Gels, Materials with Self-Assembled Fibrillar Networks, Springer, 2006.

[7] C. Guguta, I. Eeuwijk, J.M.M. Smits, R. de Gelder, Cryst. Growth Des. 8 (2008) 823–831.

[8] J.H. Wu, G. Batist, L.O. Zamir, Anti-Cancer Drug Des. 16 (2001) 129–133.

[9] J.F. Biellmann, Chem. Rev. 103 (2003) 2019–2033.

[10] M. Ibrahim-Ouali, Steroids 74 (2009) 133–162.

[11] J.N.M. Batist, A.F.M. Slobbe, A.F. Marx, Steroids 54 (1989) 321–332.

[12] A. Chatterje, B.G. Hazra, Tetrahedron 36 (1980) 2513–2519.

[13] A. Bowers, E. Denot, M.B. Sanchez, H.J. Ringold, Tetrahedron 7 (1959) 153–159.

[14] P. Forgo, I. Vincze, Steroids 67 (2002) 749–756.

[15] B. Raobaikady, A. Purohit, S.K. Chander, L.W.L. Woo, M.P. Leese, B.V.L. Potter, M.J. Reed, J. Steroid. Biochem. Mol. Biol. 84 (2003) 351–358.

[16] (a) S.K. Seth, I. Saha, C. Estarellas, A. Frontera, T. Kar, S. Mukhopadhyay, Cryst. Growth Des. 11 (2011) 3250–3265;
(b) A.L. Rohl, M. Moret, W. Kaminsky, K. Claborn, J.J. Mckinnon, B. Kahr, Cryst. Growth Des. 8 (2008) 4517–4525.

[17] M.S. Khan, O. Sulaiman, R. Hashim, M. Hemamalini, H.-K. Fun, Acta Cryst. E67 (2011), o1368.

[18] (a) Shamsuzzaman, H. Khanam, A. Mashrai, N. Siddiqui, Tetrahedron Lett. 54 (2013) 874–877;

(b) Shamsuzzaman, H. Khanam, A. Mashrai, A. Sherwani, M. Owais, N. Siddiqui, Steroids 78 (2013) 1263–1272;
(c) Shamsuzzaman, H. Khanam, A. Mashrai, M. Ahmad, Y.N. Mabkhot, W. Frey, N. Siddiqui, J. Cryst. Growth 384 (2013) 135–143;
(d) Shamsuzzaman, A. Mashrai, H. Khanam, Y.N. Mabkhot, W. Frey, J. Mol. Struct. 1063 (2014) 219–225.

[19] S.K. Wolff, D.J. Grimwood, J.J. McKinnon, D. Jayatilaka, M.A. Spackman, CrystalExplorer 2.0, University of Western Australia, Perth, Australia, 2007.

[20] W.G. Dauben, K.H. Takemura, J. Am. Chem. Soc. 75 (1953) 6302–6304.

[21] Shamsuzzaman, S. Ahmad, B.Z. Khan, Shafiullah, J. Org. Chem. 56 (1991) 1936–1937.

[22] E. Pidcock, Chem. Commun. 27 (2005) 3457–3459.

[23] F.H. Allen, O. Kennard, D.G. Watson, L. Brammer, A.G. Orpen, R.J. Taylor, Chem. Soc., Perkin Trans. 2 (1987) S1–S19.

[24] W. Kaminsky, J. Appl. Cryst. 38 (2005) 566–567.

[25] W. Kaminsky, J. Appl. Cryst. 40 (2007) 382–385.

[26] R. Hanumantharao, S. Kalainathan, G. Bhagavannarayana, U. Madhusoodanan, Spectrochim. Acta A 103 (2013) 388–399.

[27] M. Rajasekar, K. Muthu, G. Bhagavannarayana, S.P. Meenakshisundaram, J. Appl. Cryst. 45 (2012) 914–920.